Polyhedron xxx (xxxx) xxx

Contents lists available at ScienceDirect

Polyhedron

journal homepage: www.elsevier.com/locate/poly

Dual-action platinum(II) Schiff base complexes: Photocytotoxicity and cellular imaging

Samya Banerjee [a], Miles S. Capper [a], Guy J. Clarkson [a], Huaiyi Huang [a,b,*], Peter J. Sadler [a,*]

[a] Department of Chemistry, University of Warwick, Coventry CV4 7AL, UK
[b] School of Pharmaceutical Science (Shenzhen), Sun Yat-sen University, Guangzhou 510275, China

ARTICLE INFO

Article history:
Received 25 January 2019
Accepted 15 April 2019
Available online xxxx

Special Issue dedicated to Professor Akhil R. Chakravarty on the occasion of his 65th birthday

Keywords:
Platinum(II)
Schiff base
Photocytotoxicity
Cellular imaging
Singlet oxygen

ABSTRACT

Nine photo-stable Pt(II) Schiff base complexes [Pt(O^N^N^O)] (**Pt1**–**Pt9**) containing tetradentate salicylaldimine chelating ligands have been synthesized and characterized as potential photosensitisers for photodynamic therapy (PDT). The effects of electron-withdrawing versus electron-donating substituents on their electronic spectral properties are investigated. **Pt1**–**Pt9** show broad absorption bands between 400–600 nm, which makes them useful for green-light photodynamic therapy. The complexes showed intense phosphorescence with emission maxima at ca. 625 nm. This emission was used to track their cellular localization in cancer cells. Confocal cellular imaging showed that the complexes localized mostly in the cytoplasm. In the dark, the complexes were non-toxic to A549 human lung cancer cells, but exhibited high photo-toxicity upon low-dose green light (520 nm, 7.02 J/cm^2) irradiation via photo-induced singlet oxygen generation. Thus, these photoactive Pt(II) complexes have the potential to overcome the problem of drug resistance and side effects of current clinical Pt(II) drugs, and to act as both theranostic as well as therapeutic agents.

1. Introduction

Photodynamic therapy (PDT) is a non-invasive method used to treat several types of cancer as well as bacterial or fungal infections, and various skin diseases [1]. PDT requires the simultaneous presence of photosensitizers (PSs), oxygen and light [2]. Upon light activation, the PSs generate reactive oxygen species (ROS) such as singlet oxygen and hydroxyl radicals [3]. These ROS cause severe oxidative damage to biomacromolecules such as proteins and DNA in cancer cells, which triggers cell death [4]. The current clinically approved PSs such as Photofrin, Chlorin e6 and Foscan share a similar tetrapyrrolic scaffold [5]. As a result, these PSs have similar limitations in clinical use, including 1) photo-instability; 2) high tissue retention times; 3) severe skin sensitivity, and 4) side effects such as hepatitis [6,7]. Due to the 'heavy-atom effect', the introduction of a heavy metal can significantly enhance the efficiency of PDT. In recent years, metal-based tetrapyrrolic derivatives have been introduced into clinical trials as PDT agents [8,9]. For example, the Pd(II) complex, WST11 shows high absorbance at 763 nm with the 2–3× deeper light penetration depth than Photofrin [10]. However, due to the tetrapyrrolic scaffold, WST11 undergoes rapid photo-degradation which can limit its applications [11].

To overcome the above limitations, polypyridyl metal complexes have recently attracted significant attention as candidates for use in PDT with high photo-stability and enhanced aqueous solubility [12–16]. Among these complexes, TLD-1433, a Ru(II) PS has entered clinical trials for non-muscle-invasive bladder cancer [17].

On the other hand, Pt(II) complexes such as cisplatin, carboplatin, and oxaliplatin are the most widely administered anticancer drugs in clinic, but their use can be accompanied by side effects and drug resistance [18]. To overcome these restrictions, over the last decade, Pt(IV) prodrugs which undergo reduction or light-induced activation have achieved promising therapeutic effects [19,20]. The aim of the present work was to investigate novel Pt(II)-based PSs for PDT which might have fewer side effects and a different mechanism of action to circumvent resistance to Pt(II) chemotherapeutics, as well as the disadvantages of the current organic PDT agents. Recently, Pt(II) complexes have been reported as PDT agents [21–24], although Pt(II) Schiff base complexes have been rarely studied, despite their high triplet–triplet annihilation (TTA) efficiency as a result of the efficient intersystem crossing (ISC), strong visible light absorption, and high chemical and photo stability [25–28].

* Corresponding authors at: Department of Chemistry, University of Warwick, Coventry CV4 7AL, UK (H. Huang; P.J. Sadler).
E-mail addresses: huanghy87@mail.sysu.edu.cn (H. Huang), P.J.Sadler@warwick.ac.uk (P.J. Sadler).

https://doi.org/10.1016/j.poly.2019.04.024
0277-5387/

Herein, we report the synthesis, photocytotoxicity, and cellular imaging properties of nine new Pt(II) Schiff base complexes (**Pt1**–**Pt9**). Two of the complexes have been characterized by X-ray crystal structure determinations. The electronic absorption and emission properties of the complexes are discussed. The complexes have a broad visible band at ca. 400–600 nm, suitable for visible light PDT and show strong phosphorescence at ca. 625 nm with enhancement of phosphorescence in viscous and hydrophobic solvents for near-IR cellular imaging. The complexes mostly localize in the cytoplasm of cancer cells and exhibit significant photocytotoxicity, while remaining non-toxic in the dark. Overall, these complexes have potential for use in photodynamic anticancer therapy.

2. Experimental

2.1. Materials

All solvents were of analytical grade. All buffer components were of biological grade and used as received. Benzene-1,2-diamine, salicylaldehyde, and 5-methylsalicyclaldehyde, were obtained from Acros, 4,5-dimethyl-1,2-phenyleneamine, 5-fluorosalicyclaldehyde, 1,2-diamino-4,5-difluorobenzene, sulforhodamine B (SRB), Hoechst 33342, sodium acetate and K_2PtCl_4, from Sigma-Aldrich, and MitoTracker deep red FM (MTR) and LysoTracker green (LTG) from Life Technologies (USA).

2.2. Instruments and methods

2.2.1. X-ray crystallography

Single crystals of **Pt5** and **Pt9** were grown by slow vapour diffusion of diethyl ether into *N,N*-dimethylformamide solutions of **Pt5** or **Pt9**. A suitable crystal was selected and mounted on a glass fibre with Fromblin oil and placed on an Xcalibur Gemini diffractometer with a Ruby CCD area detector. The crystal was kept at 150(2) K during data collection. Using Olex2 [29], the structure was solved with the ShelXT [30] structure solution program using Intrinsic Phasing and refined with the ShelXL [31] refinement package using Least Squares minimisation. X-ray crystallographic data for **Pt5** and **Pt9** have been deposited in the CCDC under the accession numbers 1888366 and 1888367, respectively.

2.2.2. Electrochemistry

Cyclic voltammetry (CV) experiments were carried out using a CH Instrument model 600D Electrochemical Analyzer/Workstation (Austin, TX). The electrochemical measurements were performed on **Pt1**–**Pt9** (1.0 mM) in acetonitrile solutions containing tetrabutylammonium hexafluorophosphate (0.1 M) as supporting electrolyte. The solutions were degassed under nitrogen and cyclic voltammograms were scanned from −2.3 V to +2.3 V (three complete scans for each experiment). In a typical electrochemical experimental set up, the three-electrode system was used: a glassy carbon electrode as the working electrode, Ag/AgCl in 3.0 M KCl as the reference electrode, and platinum wire as the counter electrode. CV was performed at a scan rate of 100 mV/s. The excited state redox potentials were calculated from the ground state redox potentials and the emission maxima to aid evaluation of the photosensitization properties of **Pt1**–**Pt9**. Excited state reductive potentials: $E([M^*]^+/[M]^{2+}) = E_{ox} - E_{\lambda em}$, excited state oxidative potentials: $E([M^*]^+/[M]^0) = E_{red} + E_{\lambda em}$. $E_{\lambda em} = 1240/\lambda_{em}$ [32].

2.2.3. NMR, UV–Vis, phosphorescence spectroscopy, mass spectrometry (ESI-MS) and elemental analysis

^{1}H NMR spectra were acquired in 5 mm NMR tubes at 293 K or 310 K on either Bruker DPX 300 (^{1}H = 300.13 MHz) or 400 (^{1}H = 400.13 MHz) spectrometers. ^{1}H NMR chemical shifts were internally referenced to DMSO-d_6. All data processing was carried out using MestReC or TOPSPIN version 2.0 (Bruker U.K. Ltd.).

Electronic absorption spectra were recorded on a Cary 300 UV–Vis spectrophotometer using 1-cm pathlength quartz cuvettes (3 mL) and a PTP1 Peltier temperature controller. Spectra were processed using UV Winlab software. Experiments were carried out at 293 K from 600 to 200 nm.

Phosphorescence emission measurements were obtained on a JASCO FP-6500 spectrofluorometer. Complexes (10 μM) in acetonitrile were diluted from a stock solution in DMSO (1 mM). The complexes were excited at λ_{ex} = 405 nm, 465 nm and 520 nm in a 1-cm quartz cuvette at 298 K. Experiments were performed under air or nitrogen.

Electrospray ionization mass spectra were obtained by preparing the samples in 50% methanol/50% H_2O (v/v), or using NMR samples, for infusion into the mass spectrometer (Bruker Esquire 2000). The mass spectra were recorded with a scan range of *m*/*z* 400–1000 or 800–2000 for positive ions.

CHN analyses were carried out on a CE-440 elemental analyzer by Warwick Analytical (UK) Ltd.

2.2.4. Determination of singlet oxygen quantum yield

The singlet oxygen production quantum yield was determined by the N,N-dimethyl-4-nitrosoaniline/imidazole assay based on the oxidation of imidazole by singlet oxygen by following the reaction of oxidized imidazole with N,N-dimethyl-4-nitrosoaniline, as reported [33]. The absorbance of the complex was adjusted to ca. 0.1 at the irradiation wavelength. Complexes **Pt1**–**Pt9** (1 mM) in DMSO were diluted in 4 mL acetonitrile solution containing N,N-dimethyl-4-nitrosoaniline (20 μM) and imidazole (2 mM), and irradiated in 1-cm pathlength quartz fluorescence cuvettes. Bleaching of N,N-dimethyl-4-nitrosoaniline was followed by monitoring of absorbance at 520 nm. Negative control experiments were run by repetition of the measurements in the absence of imidazole. The absorbance at 420 nm was plotted as a function of irradiation time and the quantum yields of singlet oxygen formation (Φ sample) were calculated using Rose Bengal as the standard ($\Phi_{reference}$) and the following formula:

$$\Phi_{sample} = \Phi_{reference} \frac{S_{sample}}{S_{reference}} \frac{I_{reference}}{I_{sample}}$$

S represents the slope of the absorbance vs. irradiation time, I the rate of absorption calculated as the overlap of lamp emission spectra and the absorption spectra of the compound according to the following formula:

$$I = \int_{\lambda} I_0 \left[1 - 10^{-A(\lambda)}\right] d\lambda$$

where I_0 represents the light-flux intensity of the lamp and *A* is the absorbance of the compound.

2.2.5. Phosphorescence quantum yields and lifetimes

Phosphorescence quantum yields were measured on a Fluorolog spectrofluorometer (Horiba Jobin Yvon) equipped with a 405 nm pulsed diode NanoLED light source. Pt(II) complexes were diluted from a stock solution in DMSO (1 mM) to achieve an absorbance = 0.1 at 405 nm in acetonitrile. The complexes were excited at λ_{ex} = 405 nm in a 1-cm quartz cuvette at 298 K. Experiments were performed in air, and emission spectra were corrected for the spectral sensitivity of the detection system by standard correction curves. Quantum yields in aerated acetonitrile were determined by comparison with the emission of $[Ru(bpy)_3]Cl_2$ in aerated water (Φ = 0.040). Phosphorescence lifetime measurements using the same equipment and measurement procedure were continued until 1000 counts of excited state species had been

Please cite this article as: S. Banerjee, M. S. Capper, G. J. Clarkson et al., Dual-action platinum(II) Schiff base complexes: Photocytotoxicity and cellular imaging, Polyhedron, https://doi.org/10.1016/j.poly.2019.04.024

gathered. The raw data were analyzed with OriginPro 2016 software by using exponential functions to obtain the phosphorescence lifetimes.

2.2.6. Synthesis of the Schiff base ligands and corresponding Pt(II) complexes

2.2.6.1. General procedure for the synthesis of Schiff base ligands. The respective salicylaldehyde (2 mol equiv) in ethanol was added dropwise to a solution of the respective 1,2-phenyldiamines (1 mol equiv) in ethanol. The mixture was stirred overnight at room temperature. The yellow precipitate was collected and washed with cold ethanol.

Ligand 1 was obtained from benzene-1,2-diamine (216.2 mg, 2 mmol) and salicylaldehyde (488.4 mg, 4 mmol). Product: 450.6 mg of yellow powder. Yield: 67%. ^{1}H NMR (300 MHz, DMSO-d_6) δ 12.96 (s, 2H), 8.94 (s, 2H), 7.70–7.63 (m, 2H), 7.44 (ddd, J = 15.9, 7.6, 2.7 Hz, 6H), 6.98 (t, J = 7.1 Hz, 4H).

Ligand 2 was obtained from benzene-1,2-diamine (108.1 mg, 1 mmol) and 5-methylsalicyclaldehyde (272.3 mg, 2 mmol) Product: 191.6 mg of yellow powder. Yield: 55%. ^{1}H NMR (300 MHz, DMSO-d_6) δ 12.66 (s, 2H), 8.86 (s, 2H), 7.46–7.37 (m, 6H), 7.23 (dd, J = 8.4, 1.8 Hz, 2H), 6.86 (d, J = 8.4 Hz, 2H), 2.26 (s, 6H).

Ligand 3 was obtained from benzene-1,2-diamine (108.1 mg, 1 mmol) and 5-fluorosalicyclaldehyde (280.2 mg, 2 mmol). Product: 199.5 mg of yellow powder. Yield: 56%. ^{1}H NMR (300 MHz, DMSO-d_6) δ 12.61 (s, 2H), 8.91 (s, 2H), 7.53 (dd, J = 9.0, 3.1 Hz, 2H), 7.48–7.36 (m, 4H), 7.28 (td, J = 8.8, 3.2 Hz, 2H), 6.99 (dd, J = 9.0, 4.5 Hz, 2H).

Ligand 4 was obtained from 4,5-dimethyl-1,2-phenyleneamine (272.4 mg, 2 mmol) and salicyclaldehyde (488.4 mg, 4 mmol). Product: 255 mg of yellow powder. Yield: 35%. ^{1}H NMR (300 MHz, DMSO-d_6) δ 13.11 (s, 2H), 8.92 (s, 2H), 7.64 (d, J = 6.9 Hz, 2H), 7.40 (t, J = 7.2 Hz, 2H), 7.28 (s, 2H), 6.97 (t, J = 7.0 Hz, 4H), 2.29 (s, 6H).

Ligand 5 was obtained from 4,5-dimethyl-1,2-phenyleneamine (136.2 mg, 1 mmol) and 5-methylsalicyclaldehyde (272.3 mg, 2 mmol). Product: 165.6 mg of yellow powder. Yield: 44%. ^{1}H NMR (300 MHz, DMSO-d_6) δ 12.81 (s, 2H), 8.85 (s, 2H), 7.43 (s, 2H), 7.26 (s, 2H), 7.22 (d, J = 8.4 Hz, 2H), 6.85 (d, J = 8.4 Hz, 2H), 2.30 (s, 6H), 2.27 (s, 6H).

Ligand 6 was obtained from 4,5-dimethyl-1,2-phenyleneamine (136.2 mg, 1 mmol) and 5-fluorosalicyclaldehyde (280.2 mg, 2 mmol). Product: 188.3 mg yellow powder. Yield: 49%. ^{1}H NMR (300 MHz, DMSO-d_6) δ 12.74 (s, 2H), 8.91 (s, 2H), 7.52 (dd, J = 9.0, 3.0 Hz, 2H), 7.31–7.21 (m, 4H), 6.98 (dd, J = 9.0, 4.5 Hz, 2H), 2.30 (s, 6H).

Ligand 7 was obtained from 1,2-diamino-4,5-difluorobenzene (288.2 mg, 2 mmol) and salicylaldehyde (488.4 mg, 4 mmol). Product: 461.6 mg yellow powder. Yield: 62%. ^{1}H NMR (300 MHz, DMSO-d_6) δ 12.65 (s, 2H), 8.93 (s, 2H), 7.69 (dd, J = 18.5, 8.5 Hz, 4H), 7.47–7.39 (m, 2H), 6.98 (t, J = 7.5 Hz, 4H).

Ligand 8 was obtained from 1,2-diamino-4,5-difluorobenzene (144.1 mg, 1 mmol) and 5-methylsalicyclaldehyde (272.2 mg, 2 mmol). Product: 257.5 mg yellow powder. Yield: 67%.^{1}H NMR (300 MHz, DMSO-d_6) δ 12.37 (s, 2H), 8.87 (s, 2H), 7.68 (t, J = 9.9 Hz, 2H), 7.44 (s, 2H), 7.25 (d, J = 8.4 Hz, 2H), 6.87 (d, J = 8.4 Hz, 2H), 2.27 (s, 6H).

Ligand 9 was obtained from 1,2-diamino-4,5-difluorobenzene (144.1 mg, 1 mmol) and 5-fluorosalicyclaldehyde (280.2 mg, 2 mmol). Product: 294.2 mg yellow powder. Yield: 75%. ^{1}H NMR (300 MHz, DMSO-d_6) δ 12.29 (s, 1H), 8.91 (s, 1H), 7.69 (t, J = 9.9 Hz, 1H), 7.50 (dd, J = 8.9, 3.0 Hz, 1H), 7.30 (td, J = 8.7, 3.0 Hz, 1H), 7.00 (dd, J = 9.0, 4.4 Hz, 1H).

2.2.6.2. General procedure for the synthesis of platinum(II) complexes. Sodium acetate (49.2 mg, 0.6 mmol) was suspended in a solution of ligand **L1**–**L9** (0.3 mmol) in DMF (8 mL). After stirring for 5 min at room temperature, K_2PtCl_4 (124.5 mg, 1 mmol) and DMSO (4 mL) was added. The reaction mixture was heated to 343 K under nitrogen overnight. Upon cooling to room temperature, diethyl ether (40 mL) was added to afford a red precipitate. The precipitate was filtered off and washed with water, acetone and diethyl ether, and dried under vacuum.

Pt1: 70.3 mg of red precipitate. Yield: 46%. ^{1}H NMR (300 MHz, DMSO-d_6) δ 9.55 (s, 1H), 8.47 (dd, J = 6.1, 3.4 Hz, 1H), 7.88 (d, J = 8.1 Hz, 1H), 7.61–7.32 (m, 2H), 7.13 (d, J = 8.5 Hz, 1H), 6.82 (d, J = 7.8 Hz, 1H). *Anal.* Calc. for $C_{20}H_{14}N_2O_2Pt$: C, 47.15; H, 2.77; N, 5.50. Found: C, 47.33; H, 2.91; N, 5.41. ESI-MS: m/z $[M+Na]^+$ 533.4, $[2M+Na]^+$ 1041.0, $[3M+Na]^+$ 1551.2.

Pt2: 56.4 mg of red precipitate. Yield: 35%. ^{1}H NMR (300 MHz, DMSO-d_6) δ 9.46 (s, 2H), 8.44 (dd, J = 6.3, 3.3 Hz, 2H), 7.65 (s, 2H), 7.44 (dd, J = 11.7, 5.7 Hz, 4H), 7.04 (d, J = 8.7 Hz, 2H), 2.30 (s, 6H). *Anal.* Calc. for $C_{22}H_{18}N_2O_2Pt$: C, 49.16; H, 3.38; N, 5.21. Found: C, C, 49.02; H, 3.47; N, 5.35. ESI-MS: m/z $[M+Na]^+$ 561.0, $[2M+Na]^+$ 1098.1.

Pt3: 41.0 mg of red precipitate. Yield: 31%. ^{1}H NMR (300 MHz, DMSO-d_6) δ 9.57 (s, 1H), 8.42 (dd, J = 6.1, 3.3 Hz, 1H), 7.76–7.32 (m, 3H), 7.13 (dd, J = 9.4, 4.8 Hz, 1H). *Anal.* Calc. for $C_{20}H_{12}F_2N_2O_2$-Pt: C, 44.04; H, 2.22; N, 5.14. Found: C, 43.87; H, 2.26; N, 5.32. ESI-MS: m/z $[M+Na]^+$ 568.4, $[2M+Na]^+$ 1113.0, $[3M+Na]^+$ 1658.4.

Pt4: 49.8 mg of red precipitate. Yield: 31%. ^{1}H NMR (300 MHz, DMSO-d_6) δ 9.43 (s, 2H), 8.23 (s, 2H), 7.84 (d, J = 6.6 Hz, 2H), 7.55 (s, 2H), 7.10 (d, J = 8.5 Hz, 2H), 6.77 (s, 2H), 2.35 (s, 6H). *Anal.* Calc. for $C_{22}H_{18}N_2O_2Pt$: C, 49.16; H, 3.38; N, 5.21. Found: C, 48.87; H, 3.21; N, 5.33. ESI-MS: m/z $[M+Na]^+$ 561.0, $[2M+Na]^+$ 1098.0, $[3M+Na]^+$ 1637.1.

Pt5: 59.4 mg of red precipitate. Yield: 35%. ^{1}H NMR (300 MHz, DMSO-d_6) δ 9.35 (s, 2H), 8.21 (s, 2H), 7.60 (s, 2H), 7.39 (d, J = 9.0 Hz, 2H), 7.01 (d, J = 8.7 Hz, 2H), 2.35 (s, 6H), 2.29 (s, 6H). ^{13}C NMR (126 MHz, DMF-d_6) δ 163.67, 150.08, 143.32, 137.10, 136.95, 134.13, 124.65, 121.96, 121.25, 116.89, 19.36, 19.22. *Anal.* Calc. for $C_{24}H_{22}N_2O_2Pt$: C, 50.97; H, 3.92; N, 4.95. Found: C, 51.35; H, 3.78; N, 4.96.ESI-MS: m/z $[M+Na]^+$ 588.1, $[2M+Na]^+$ 1153.1, $[3M+Na]^+$ 1720.2.

Pt6: 77.4 mg of red precipitate. Yield: 45%. ^{1}H NMR (300 MHz, DMSO-d_6) δ 9.33 (s, 1H), 8.07 (s, 1H), 7.55 (d, J = 9.5 Hz, 1H), 7.45 (t, J = 7.7 Hz, 1H), 7.07 (dd, J = 9.3, 4.7 Hz, 1H), 2.28 (s, 3H). ^{13}C NMR (126 MHz, DMSO-d_6) δ 161.46, 154.25, 152.41, 150.33, 143.00, 137.66, 124.20, 122.84, 121.13, 118.10, 117.38, 20.04. *Anal.* Calc. for $C_{22}H_{16}F_2N_2O_2Pt$: C, 46.08; H, 2.81; N, 4.89. Found: C, 45.64; H, 2.66; N, 4.86. ESI-MS: m/z $[M+Na]^+$ 595.0, $[2M+Na]^+$ 1169.0, $[3M+Na]^+$ 1743.0.

P7: 57.2 mg of red precipitate. Yield: 34%. ^{1}H NMR (300 MHz, DMSO-d_6) δ 9.34 (s, 2H), 8.57 (t, J = 9.8 Hz, 2H), 7.75 (d, J = 7.1 Hz, 2H), 7.57 (t, J = 7.0 Hz, 2H), 7.09 (d, J = 8.6 Hz, 2H), 6.77 (t, J = 7.2 Hz, 2H). ^{13}C NMR (126 MHz, DMSO-d_6) δ 161.46, 154.25, 152.41, 150.33, 143.00, 137.67, 124.20, 122.85, 121.13, 118.10. *Anal.* Calc. for $C_{20}H_{12}F_2N_2O_2Pt$: C, 44.04; H, 2.22; N, 5.14. Found: C, 43.81; H, 2.05; N,5.02. ESI-MS: m/z $[2M+Na]^+$ 1113.0, $[3M+Na]^+$ 1659.0.

Pt8: 63.6 mg of red precipitate. Yield: 37%. ^{1}H NMR (300 MHz, DMSO-d_6) δ 9.33 (s, 2H), 8.62 (d, J = 10.2 Hz, 2H), 7.55 (s, 2H), 7.43 (d, J = 8.7 Hz, 2H), 7.04 (d, J = 8.7 Hz, 2H), 2.29 (s, 6H). ^{13}C NMR (126 MHz, DMSO-d_6) δ 163.48, 152.15, 151.12, 149.5, 147.6, 141.79, 138.08, 134.54, 125.14, 121.74, 121.61, 20.16. *Anal.* Calc. for $C_{22}H_{16}F_2N_2O_2Pt$: C, 46.08; H, 2.81; N, 4.89. Found: C, 45.88; H, 2.69; N, 4.83. ESI-MS: m/z $[2M+Na]^+$ 1171.1, $[3M+Na]^+$ 1744.0.

Pt9: 97.7 mg of red precipitate. Yield: 56%. ^{1}H NMR (300 MHz, DMSO-d_6) δ 9.37 (s, 2H), 8.52 (t, J = 9.8 Hz, 2H), 7.51 (d, J = 8.7 Hz, 4H), 7.13 (s, 2H). ^{13}C NMR (126 MHz, DMF-d_6) δ 154.49, 152.65, 151.65, 141.84, 128.41, 124.65, 123.04, 120.81, 117.55, 105.29. *Anal.* Calc. for $C_{20}H_{10}F_4N_2O_2Pt$: C, 41.32; H, 1.73;

Please cite this article as: S. Banerjee, M. S. Capper, G. J. Clarkson et al., Dual-action platinum(II) Schiff base complexes: Photocytotoxicity and cellular imaging, Polyhedron, https://doi.org/10.1016/j.poly.2019.04.024

N, 4.82. Found: C, 41.77; H, 2.05; N, 5.49. ESI-MS: *m/z* $[2M+Na]^+$ 1185.0, $[3M+Na]^+$ 1766.9.

2.2.7. Cell culture and cell assays

2.2.7.1. Cell culture. The cisplatin-sensitive human lung carcinoma cell line A549 and cisplatin-resistant human lung carcinoma cell line A549R were obtained from the European Collection of Cell Cultures (ECACC) and used between passages 5 to 18. Cells were grown in Roswell Park Memorial Institute medium (RPMI-1640) supplemented with 10% fetal calf serum and 1% penicillin and streptomycin. To maintain the resistant phenotype, A549R cells were incubated with 5 μM cisplatin and cultured in drug-free medium for at least a week before use. The cells were grown as adherent monolayers at 310 K in a 5% CO_2 humidified atmosphere and passaged at ca. 70–80% confluence.

2.2.7.2. Dark- and photo-cytotoxicity assays. 5000 A549 cells were seeded per well in 96-well plates at 310 K in a 5% CO_2/95% air incubator (Thermo) for 24 h. Stock solutions of the test compounds were firstly prepared in 5% DMSO (v/v) and a mixture 0.9% saline and RPMI-1640 medium (1:1 v/v) following serial dilutions in RPMI-1640. The drug exposure period was 4 h. After this, supernatants were removed by suction and each well was washed with PBS. For light treatment, the cells were then irradiated in phenol-red-free cell culture medium by 520 nm light (7.02 J cm^{-2}). Then the cells were allowed to recover for a further 44 h in the incubator at 310 K. For dark-treated cells, after drug exposure, the cells were incubated in drug-free cell culture medium at 310 K for 44 h. Finally, the cytotoxicity was determined by sulforhodamine B (SRB) assay on a GloMax-Multi Microplate Multimode Reader. IC_{50} values were determined as duplicates of triplicates in two independent sets of experiments and their standard deviations were calculated.

2.2.7.3. Cellular localization assays. A549 cells were seeded in a glass-bottom dish (35 mm dish with 20 mm bottom well (Costar) at 310 K in a 5% CO_2/95% air incubator. The cells were incubated with **Pt1**–**Pt9** (5 μM) at 310 K for 4 h and further stained with 100 μM MTR and LTR or Hoechst 33,342 Cell imaging was carried out immediately by confocal microscopy (LSM 710, Carl Zeiss, Göttingen, Germany) with a 63 × oil-immersion objective lens. Excitation/emission: **1** one-photon 405/562 nm and two-photon 760/562 nm, LTG 488/520 nm, MTR 633/660 nm.

3. Results and discussion

3.1. Synthesis and characterization

To investigate the relationship between the photophysical, photochemical and photobiological activity of the Pt(II) Schiff base complexes, we designed and synthesized complexes **Pt1**–**Pt9** (Scheme 1) with either electron-withdrawing or electron-donating groups at R^1 or R^2 positions on the backbone phenyl ring. Schiff base ligands **H_2L1**–**H_2L9** were synthesised by amine-aldehyde condensation reactions from disubstituted (–H, $–CH_3$, –F) o-phenylenediamine and substituted (–H, $–CH_3$, –F) salicylaldehyde in ethanol at room temperature. All the ligands were characterised by ^{1}H NMR and mass spectra.

Pt(II) complexes **Pt1**–**Pt9** (Scheme 1) were synthesised by heating the Schiff base ligand, sodium acetate and K_2PtCl_4 in DMSO and DMF (1:1 v/v) at 343 K overnight. All the complexes were characterised by ^{1}H, ^{13}C, COSY NMR, elemental analysis and mass spectrometry. The disappearance of the aromatic OH ^{1}H NMR signal (between 12 and 13 ppm) indicated the coordination of the ligand to Pt(II). The presence of fluorine at the R^1 position strongly influenced the ^{1}H NMR peak splitting patterns. For instance, **Pt7** showed a triplet peak at 8.57 but without any proton coupling, confirmed by the COSY NMR (Fig. S1, SI). Thus the splitting of this proton signal was due to ^{19}F coupling. Complexes were further characterized by mass spectral data showing peaks corresponding to $[2M+Na]^+$ and $[3M+Na]^+$.

3.1.1. X-Ray crystallography

Crystals of **Pt5** and **Pt9** (Fig. 1, Table S1) suitable for X-ray diffraction were obtained via diffusion of ethyl ether into DMF solutions of the complexes. The complexes crystallized in the monoclinic space groups $P2_1/n$ and $P2_1/c$, respectively, with four molecules in the unit cell. They are discrete mononuclear species with a PtN_2O_2 core formed by the tetradentate O^N^N^O-donor Schiff base in a distorted square-planar environment. Pt-O bond distances are similar in both the complexes (ca. 1.99 Å), slightly longer than the Pt-N bond distances (ca. 1.96 Å, Table S2). Both the Pt–O and Pt–N bond distance lies in the range of the previous literature reports [22,23].

3.1.2. Photochemical and photophysical properties

The convenient structural modifications and facile synthesis of ligands made it possible to study the structure–activity relation-

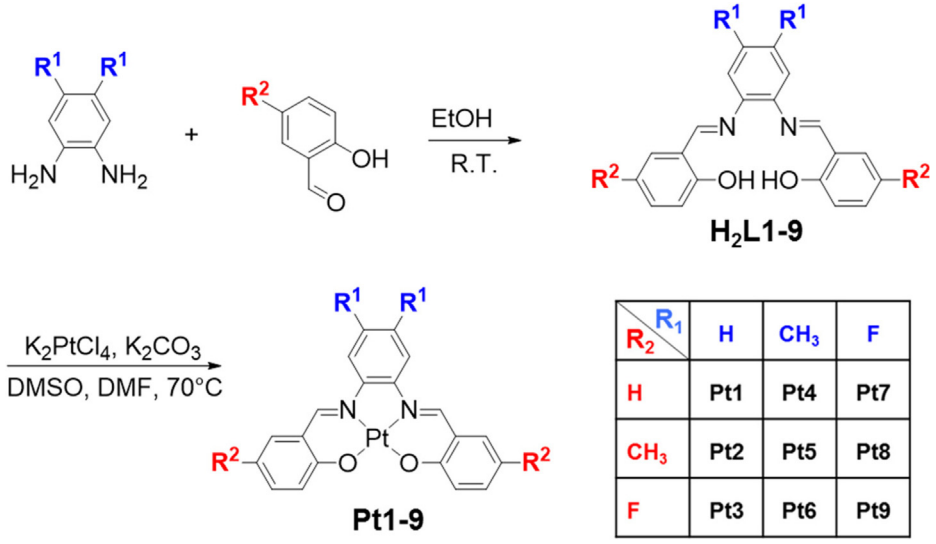

R2 \ R1	H	CH_3	F
H	Pt1	Pt4	Pt7
CH_3	Pt2	Pt5	Pt8
F	Pt3	Pt6	Pt9

Scheme 1. Synthetic route for the Schiff base ligands **H_2L1**–**9** and Pt(II) complexes **Pt1**–**Pt9**.

Please cite this article as: S. Banerjee, M. S. Capper, G. J. Clarkson et al., Dual-action platinum(II) Schiff base complexes: Photocytotoxicity and cellular imaging, Polyhedron, https://doi.org/10.1016/j.poly.2019.04.024

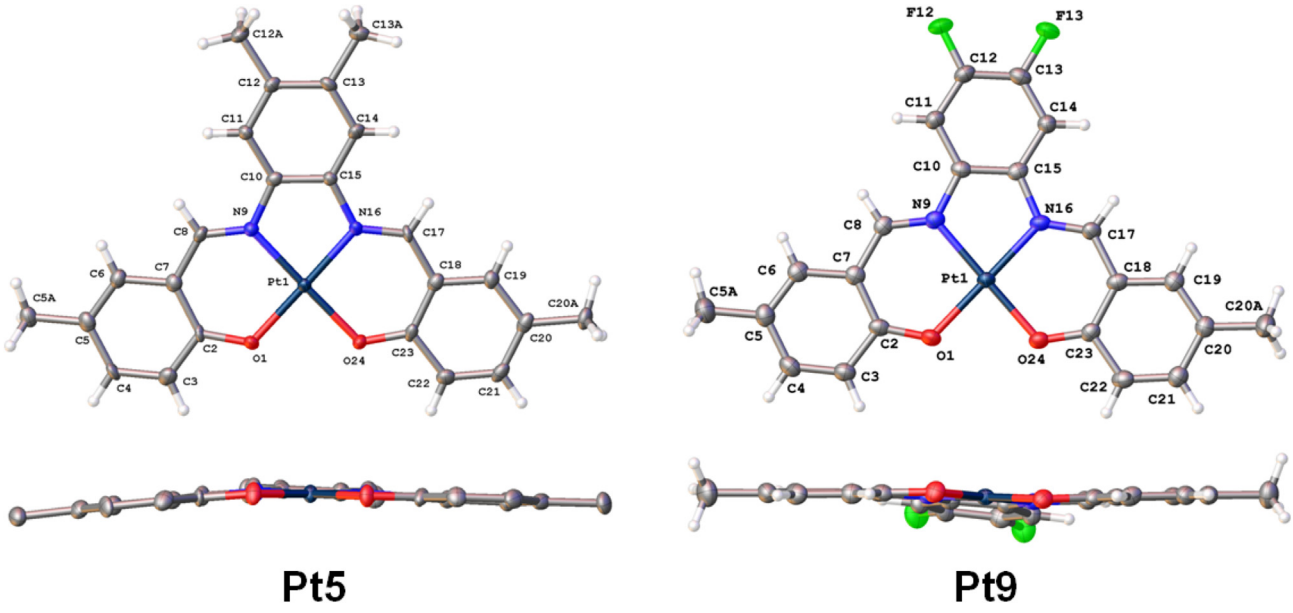

Fig. 1. Side and top views of the X-ray crystal structures of complexes **Pt5** and **Pt9** with 50% thermal ellipsoids.

ships for 9 Schiff base-Pt(II) complexes. The UV–vis absorption spectra of **Pt1**–**Pt9** in acetonitrile are shown in Fig. 2. All the solutions of Pt(II) complexes in MeCN were red in colour with similar absorption spectral features between 200 and 600 nm. The intense absorption band at around 260 nm is assignable to the Schiff base ligands, and those near 310 nm are π–π^* ligand-based transitions [34]. The two strong absorption bands between 350 and 400 nm are assignable to a mixture of metal-to-ligand $^1[Pt^{II} \rightarrow \pi^*\text{-}(L)]$ transitions [34]. The absorption bands in the visible range (420–600 nm) are metal-to-ligand-charge-transfer (MLCT) bands [25].

The substituents (CH_3 or F) have a significant influence on the electronic absorption spectra. For **Pt1**, **Pt4** and **Pt7** with different substituents at the R^1 position, $-CH_3$ induced a hypsochromic effect (3 nm, in **Pt4**) and –F induced a bathochromic effect (4 nm, in **Pt7**) compared with –H atom (in **Pt1**). For substitution at the R^2 position, both the $-CH_3$ (15 nm, in **Pt2**) and –F (23 nm, in **Pt3**) groups induced bathochromic effects compared to **Pt1**. This larger red-shift of **Pt3** (ca 20 nm) compared with **Pt7** (4 nm) indicates that –F substitution at R^2 significantly extends the absorption to longer wavelength. **Pt9,** where both R^1 and R^2 are –F, exhibited

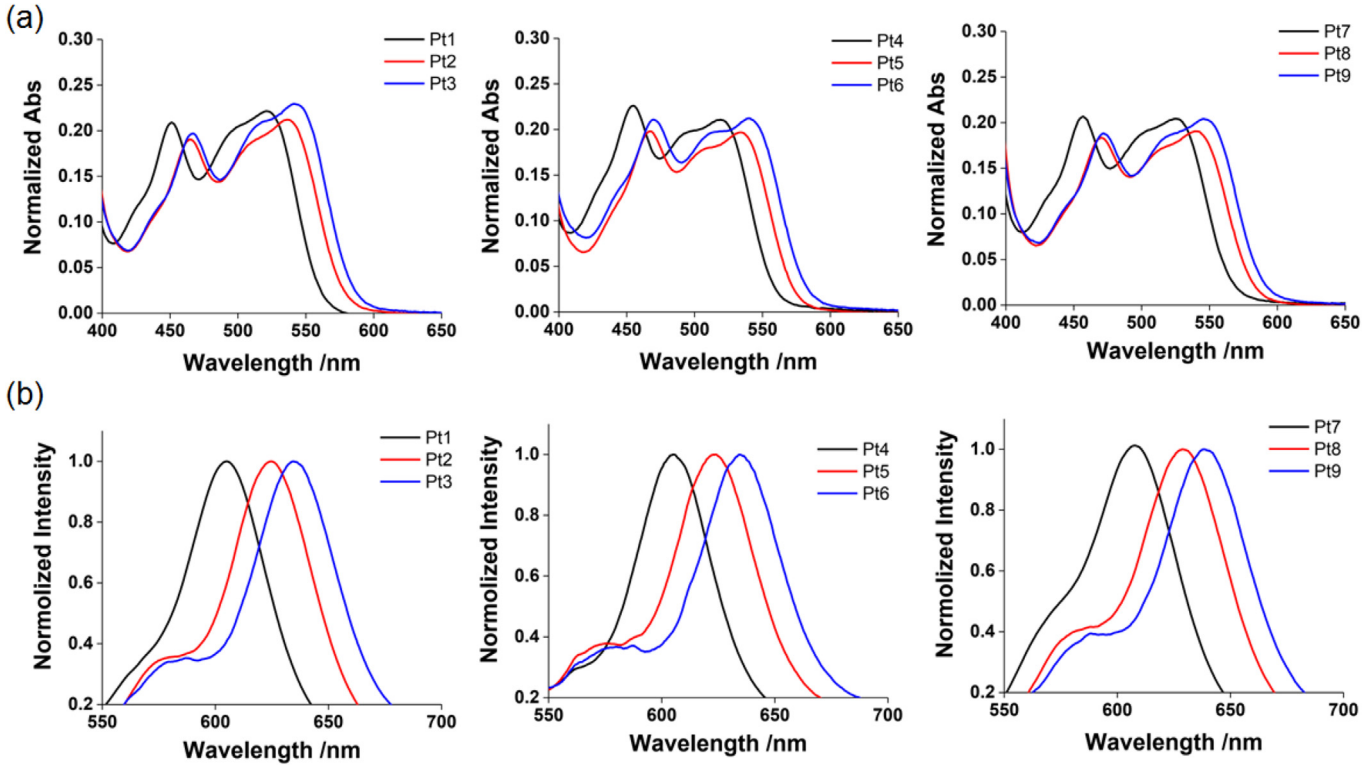

Fig. 2. The effect of substituents on (a) the UV–Vis spectra of **Pt1**–**Pt9** (10 μM) in acetonitrile, and b) normalized emission spectra of **Pt1**–**Pt9** (10 μM) in acetonitrile. E_x = 520 nm.

Please cite this article as: S. Banerjee, M. S. Capper, G. J. Clarkson et al., Dual-action platinum(II) Schiff base complexes: Photocytotoxicity and cellular imaging, Polyhedron, https://doi.org/10.1016/j.poly.2019.04.024

26 nm bathochromic shift compared with **Pt1** and as a result, the spectrum tail of **Pt9** extended up to 600 nm which is ideal for near-IR light PDT [35]. Interestingly, **Pt4** and **Pt5** showed significant hypochromic effects and their molar extinction coefficients are much smaller than those for the other Pt(II) complexes.

3.1.3. Oxygen and viscosity sensitivity

Phosphorescence spectra of **Pt1**–**Pt9** were recorded in acetonitrile at ambient temperature. Since all the Pt(II) complexes exhibit strong absorption across the whole visible range, the wavelength dependence of phosphorescence was investigated. Three excitation wavelengths were selected: 405 nm, 465 nm and 520 nm. As shown in Fig. 3, **Pt1**–**Pt9** (10 μM) all exhibited red phosphorescence between 604 and 644 nm. The highest emission intensity was obtained with excitation at 520 nm.

Similar to the UV–Vis absorption spectra, substitution at the R^1 or R^2 position also influenced the emission spectra (Fig. 3). **Pt1**, **Pt4** and **Pt7** displayed the most blue-shifted emission maximum at 604, 607 and 609 nm, respectively, compared with R^2-substituted complexes. Substitution with either $-CH_3$ or –F group at R^2 significantly shifted the emission maximum to longer wavelength (e.g. **Pt1** 604 nm, **Pt2** 625 nm, **Pt3** 633 nm) while the –F substituent showed a more effective red-shift than $-CH_3$. Taking the emission and the UV–Vis data into consideration, it is apparent that a substituent at the R^2 position has a stronger effect on the emission and absorbance properties of Pt(II) Schiff base complexes than the R^1 position.

The emission spectra were recorded under N_2 in acetonitrile to investigate the effect of oxygen on the emission. As shown in Fig. 3a and b, the emission intensity of all the Pt(II) complexes under a nitrogen environment increased significantly compared to the intensity measured under air. **Pt2** was the most oxygen-sensitive complex with a 32× phosphorescence enhancement under nitrogen (Fig. 3c). **Pt1** showed the smallest emission enhancement (8×) among all the Pt(II) complexes while it exhibited strongest emission in air. The phosphorescence of the complexes can be used to track the complexes inside cells by cellular imaging. Moreover, upon introducing functional groups, the phosphorescence intensity of **Pt7** showed a better linear relationship with increasing concentration than **Pt1** (Fig. 3d). Thus the functional groups may introduce steric hindrance which might obstruct π–π stacking between the planar Pt(II) complexes.

3.1.4. Effect of solvent polarity and viscosity

The influence of polarity and viscosity on the emission of the complexes Pt**1**–**9** is important for the possible use of these complexes as cellular imaging or PDT agents since the intracellular microenvironment is complicated with areas of varied polarity and viscosity [36]. As shown in Fig. 4 b, solvent polarity has only a little effect on the emission intensities. However, the viscosity of the solvent has a strong influence. The phosphorescence intensity was much higher in viscous solvents like glycerol compared to the other low viscosity solvents as depicted in Fig. 4a,b. Furthermore, at different percentages of glycerol/water the phosphorescence intensity was enhanced significantly with increased percentage of glycerol. Complex Pt**7**, in particular displayed the highest intensity enhancement in the presence of glycerol compared with all other Pt(II) complexes. The phosphorescence lifetime of **Pt7** in acetonitrile and glycerol indicated (Fig. 4a) that Pt**7** has a more than 40x longer excited-state lifetime time in glycerol (3277 ns) than in acetonitrile (80.7 ns). These results indicate that high viscosity and hydrophobic environments enhance the phosphorescence intensity of these Pt(II) Schiff base complexes.

3.1.5. Cyclic voltammetry

Cyclic voltammograms of **Pt1**–**Pt9** were recorded in degassed DMF (1 mM) with 100 mM tetrabutylammonium hexafluorophosphate (TBAP) as supporting electrolyte. All potentials are refer-

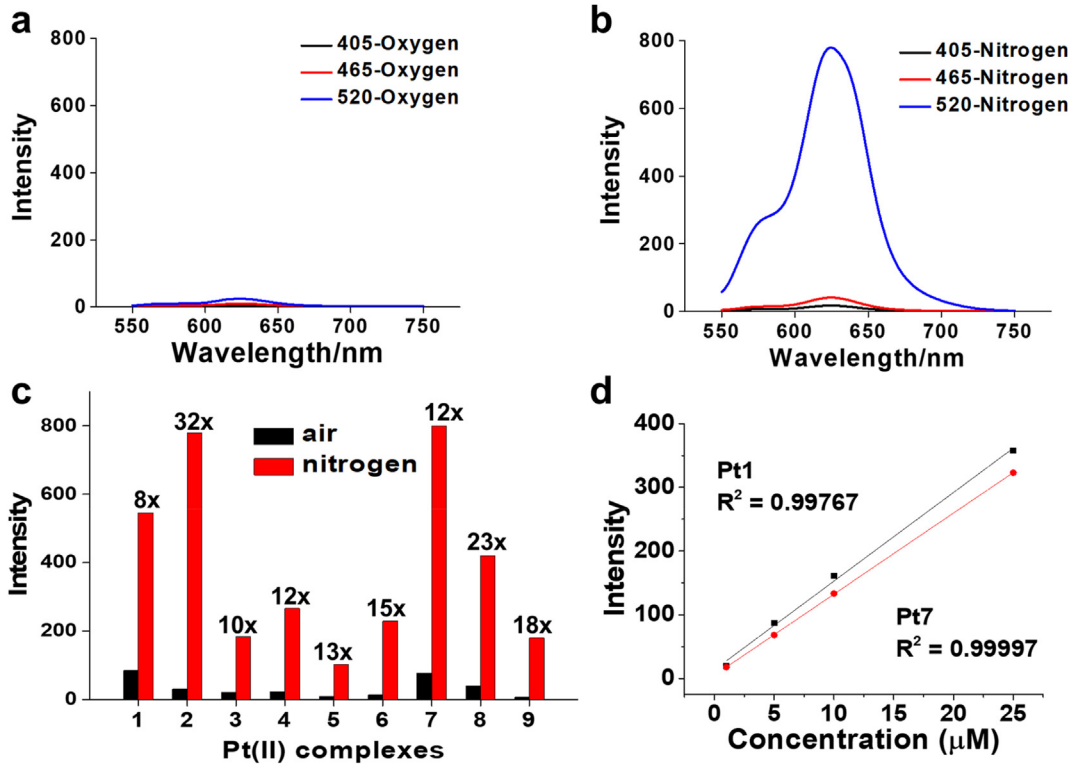

Fig. 3. (a) Emission spectra of **Pt2** (10 μM) in acetonitrile in air. (b) Emission spectra of **Pt2** (10 μM) under nitrogen. (c) Comparison of emission intensity of **Pt1**–**9** (10 μM) in air and under nitrogen. (d) Concentration dependent phosphorescence intensity of **Pt1** (black) and **Pt7** (red) in air-saturated acetonitrile. (Colour online.)

Please cite this article as: S. Banerjee, M. S. Capper, G. J. Clarkson et al., Dual-action platinum(II) Schiff base complexes: Photocytotoxicity and cellular imaging, Polyhedron, https://doi.org/10.1016/j.poly.2019.04.024

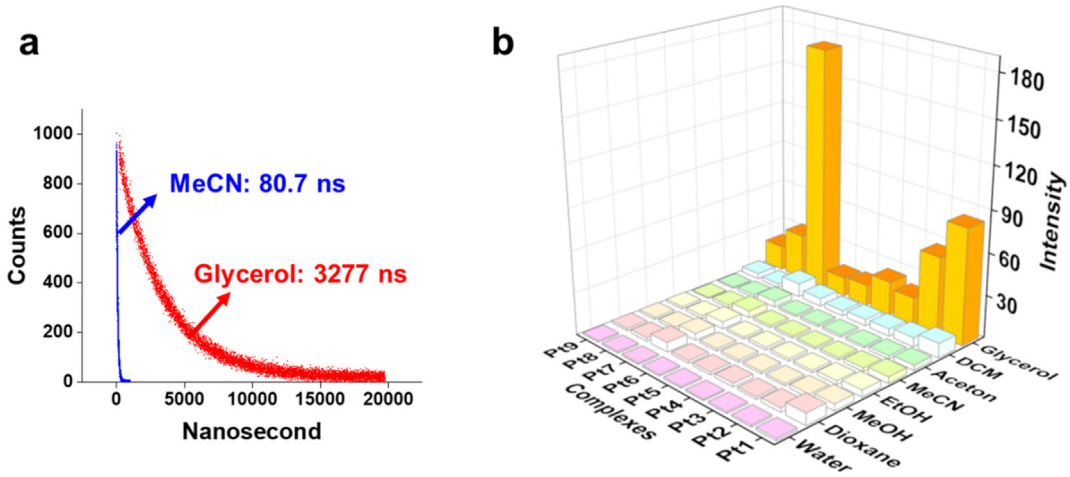

Fig. 4. (a) Excited state lifetime measurement for **Pt7** in air-saturated acetonitrile and glycerol. (b) Emission intensity of **Pt1**–**Pt9** (3 μM) in solvents of varying polarity and viscosity.

enced to the ferrocenium–ferrocene [$E°(FeCp_2^{+/0})$] couple. In each case, there is one irreversible anodic peak with E_{pa} at 0.424–0.687 V and one irreversible cathodic peak with E_{pc} at −1.733 to −2.019 V (Fig. S2). The anodic and cathodic peaks are attributed to the oxidation and reduction of Schiff base ligands, respectively [25]. Introduction of the –CH_3 group reduced the oxidation potential, while –F increased both the oxidation and reduction potentials in all of the complexes. The excited-state redox potentials of the complexes were determined in order to assess the photosensitization properties of the complexes (Table 1). Upon excitation by green light, these Pt(II) Schiff base complexes became more reductive rather than oxidative.

3.1.6. Singlet oxygen generation

The highly oxygen-sensitive emission of the Pt(II) complexes indicates that the complexes probably interact with $^3O_2$ in their excited states and may generate singlet oxygen ($^1O_2$) upon photo-excitation. Thus the singlet oxygen quantum yields of **Pt1**–**Pt9** were determined in acetonitrile using both indirect and direct methods. The indirect method tracks the photo bleaching of N,N-dimethyl-4-nitrosoaniline (RNO) induced by imidazole and singlet oxygen over time. The direct method records the laser power dependence of near infrared singlet oxygen phosphorescence spectra, with Rose Bengal as a reference photosensitizer.

Singlet oxygen phosphorescence spectra with emission maximum at 1270 nm were observed for all the Pt(II) complexes (Fig. 5a,b). **Pt3**, **Pt6** and **Pt7** with **–**F substitution showed relatively higher singlet oxygen quantum yields of 46%, 43% and 42%, respectively. Previous studies also showed that the presence of a fluorine substituent increases the antitumor effects with enhanced singlet oxygen generation [37,38]. These Pt(II) complexes exhibited excellent photostability and solubility in acetonitrile during photo-irradiation, making them suitable as PDT agents.

Table 1
Electrochemical properties of **Pt1**–**Pt9** and their calculated excited-state redox potentials.

Complexes	Ground State		Excited State	
	E_{pa}/V	E_{pc}/V	$^*E(M/[M]^+)$/V	$^*E(M/[M]^-)$/V
Pt1	0.581	−1.946	−1.471	0.106
Pt2	0.456	−1.982	−1.528	0.002
Pt3	0.525	−1.827	−1.433	0.131
Pt4	0.517	−1.997	−1.525	0.045
Pt5	0.424	−2.019	−1.556	−0.038
Pt6	0.612	−1.857	−1.337	0.092
Pt7	0.648	−1.873	−1.388	0.163
Pt8	0.517	−1.911	−1.467	0.073
Pt9	0.687	−1.733	−1.238	0.192

3.1.7. Cell imaging and cellular localization

Based on the unique phosphorescence property of the complexes, confocal microscopy imaging of **Pt1**–**Pt9** treated living A549 lung cancer cells under 520 nm excitation was carried out to track the complexes inside cancer cells. As shown in Fig. 6, under 520 nm excitation, **Pt1**–**Pt3** showed much stronger intracellular phosphorescence than the other Pt(II) complexes, especially **Pt7**–**Pt9** whose intracellular phosphorescence was too weak to detect. From the cell imaging data, it was evident that the Pt(II) complexes have similar intracellular localization, mostly in the cytoplasm. Subsequently, to confirm whether these Pt(II) complexes can target specific organelles in the cytoplasm, **Pt1** was selected for co-staining with commercial organelle dyes due to its strongest intracellular phosphorescence intensity. A549 lung cancer cells were firstly incubated with **Pt1** (5 μM, 4 h) and then with specific organelle dyes (30 min) in the dark, and finally imaged with a confocal microscope. As shown in Fig. 7, the red signal of **Pt1** overlayed with both the fluorescence signal of Mitotracker green (mitochondrion-staining dye) and of Lysotracker green (lysosome-imaging dye). No overlay of luminescence was observed with the nucleus-staining dye Hoechst 33342. All these data indicate that these Pt(II) complexes target cell mitochondria and lysosomes rather than the cell nucleus. Clinically approved Pt(II) drugs such as cisplatin and carboplatin are known to target the cell nucleus and cross-link nuclear DNA [39]. Resistance to these Pt drugs occurs due to the repair of such platinum-DNA cross links by a nucleotide excision repair mechanism [40]. Hence these mitochondrion- and lysosome-targeting complexes could provide a novel mechanism of anticancer activity to overcome Pt-drug resistance.

3.1.8. Photocytotoxicity

After confirming the intracellular internalization and specific distribution of complexes **Pt1**–**9** in A549 cancer cells, we explored the anticancer activity of these complexes, particularly as PDT agents considering their excellent ability to generate $^1O_2$. The anticancer activity of these complexes was studied both in the dark and upon light irradiation. As shown in Table 2, all the Pt(II) complexes were non-toxic in A549 cancer cells in the dark up to 20 μM concentration, the cell survival percentages were all >80% after 4 h drug exposure followed by 44 h recovery. However, upon irradiation with a low dose of 520 nm green light (7.02 J/cm^2), significant photo-toxicity was observed, with several giving nanomolar IC_{50}

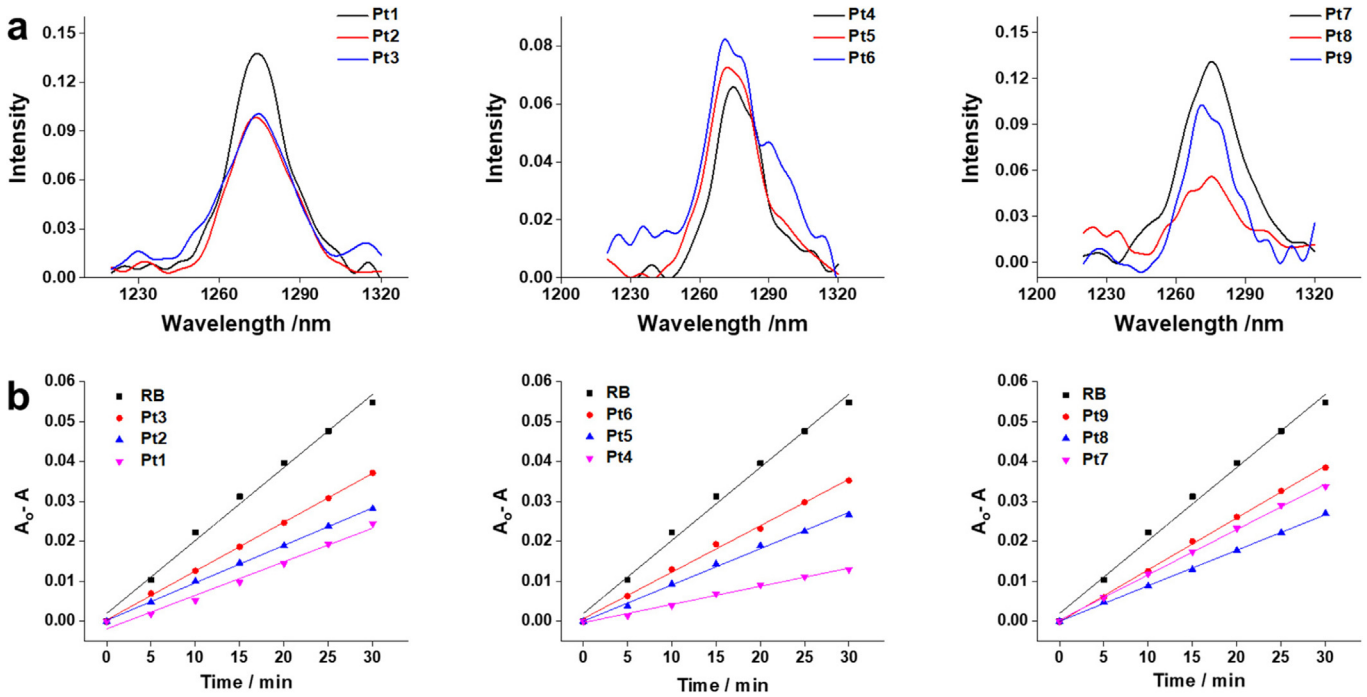

Fig. 5. a) Near-infrared singlet oxygen signal generated by **Pt1**–**Pt9** after irradiation with 520 nm light in acetonitrile. b) Singlet oxygen generation quantum yields measured from the absorption attenuation ($\Delta A = A_0 - A_t$) of RNO under 520 nm light exposure in acetonitrile. The slope corresponds to the absolute amount of generated $^1O_2$.

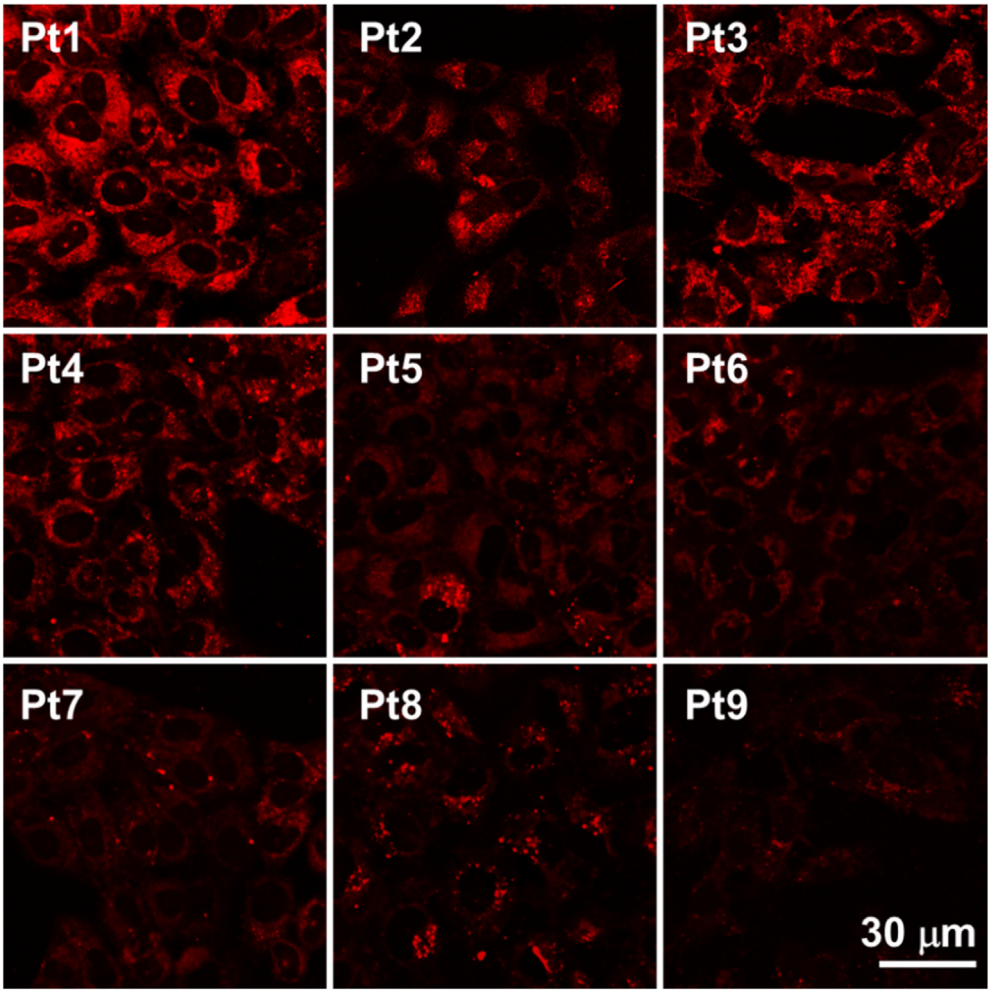

Fig. 6. Live A549 lung cancer cell imaging with the Pt(II) Schiff base complexes. Excitation wavelength: 520 nm. Emission filter: 600 ± 40 nm.

Please cite this article as: S. Banerjee, M. S. Capper, G. J. Clarkson et al., Dual-action platinum(II) Schiff base complexes: Photocytotoxicity and cellular imaging, Polyhedron, https://doi.org/10.1016/j.poly.2019.04.024

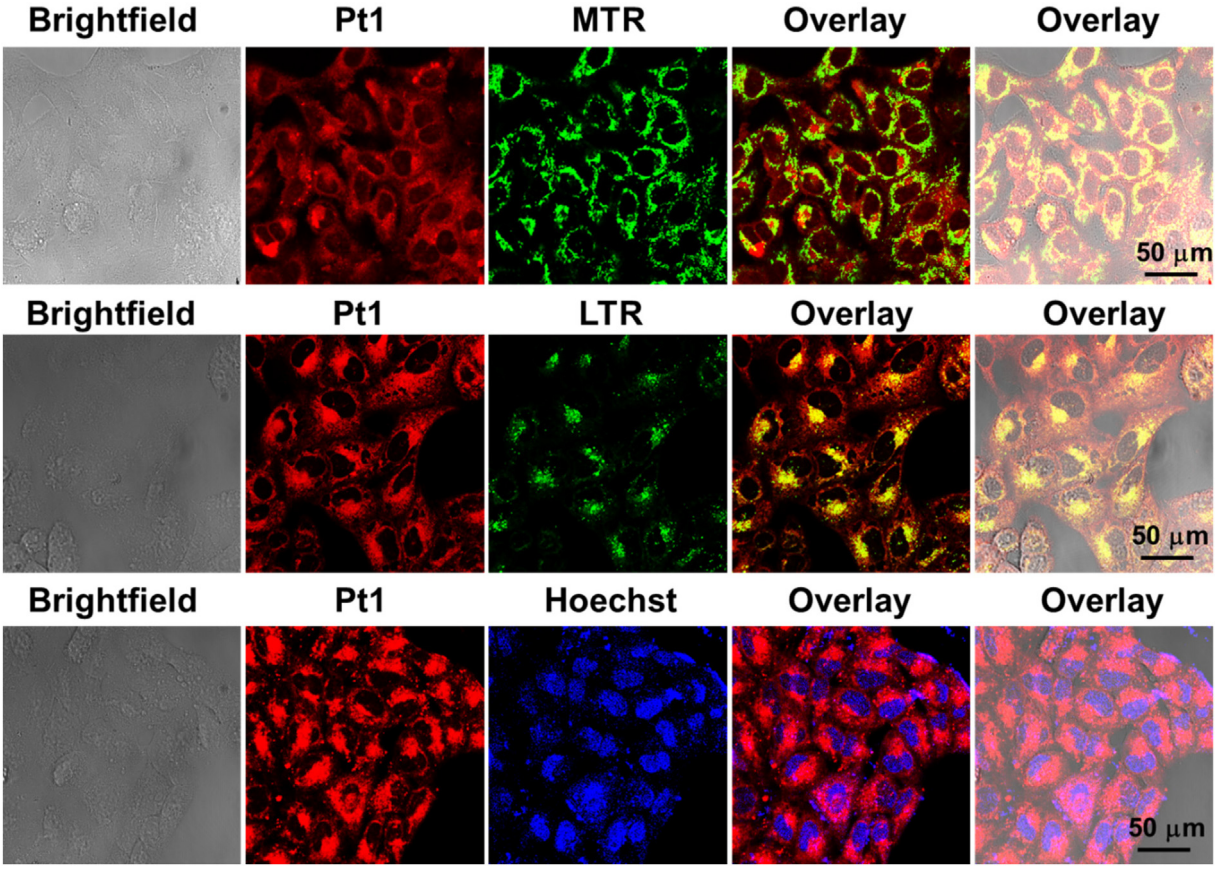

Fig. 7. Intracellular localization of **Pt1** in A549 lung cancer cells. A549 cells were firstly incubated with **Pt1** (5 μM, 4 h), and then with commercial dyes for another 30 min. Scale bar = 50 μm. Excitation wavelengths: 520 nm for **Pt1**, 488 nm for Mitotracker and Lysotracker, 405 nm for Hoechst 33342. Emission filter: 600 ± 20 nm for Pt(II) complexes, 520 ± 20 nm for Mitotracker and Lysotracker, 460 ± 20 nm for Hoechst 33342.

Table 2
Dark- and photo-toxicity of **Pt1**–**Pt9** towards A549 and cisplatin-resistant A549R lung cancer cells (IC_{50}/μM).

Cell line	A549			A549R		
Compound	Dark[a]	Light[a]	PI	Dark[a]	Light[a]	PI
Pt1[a]	>20	0.20 ± 0.015	>100	>20	0.30 ± 0.010	>66
Pt2[a]	>20	0.13 ± 0.007	>159	>20	0.12 ± 0.011	>166
Pt3[a]	>20	0.21 ± 0.025	>98	>20	0.35 ± 0.023	>57
Pt4[a]	>20	0.15 ± 0.010	>134	>20	0.23 ± 0.015	>87
Pt5[a]	>10	1.50 ± 0.021	>7	n.d.	n.d.	n.d.
Pt6[a]	>10	8.05 ± 0.69	>1	n.d.	n.d.	n.d.
Pt7[a]	>20	0.37 ± 0.025	>55	n.d.	n.d.	n.d.
Pt8[a]	>10	>10	n.a.	n.d.	n.d.	n.d.
Pt9[a]	>10	>10	n.a.	n.d.	n.d.	n.d.
Cisplatin[a]	55.6 ± 6.3	54.7 ± 4.4	n.a.	>200	>200	n.d.
Cisplatin[b]	4.6 ± 0.5	4.7 ± 0.3	n.a.	32.4 ± 3.5	34.0 ± 2.9	n.d.
5-ALA	>200	>200	n.a.	>200	>200	n.d.

[a] The drug exposure time was 4 h. The cells were washed, replaced with fresh cell culture medium and then received dark or light (520 nm, 7.02 J/cm^2) treatment followed by 44 h recovery.
[b] The drug exposure time was 48 h. n.d.: not detected. n.a.: not available.

values. **Pt2**–**Pt5** exhibited much better phototoxicity than **Pt1** (which contained no substituents).

4. Conclusions

A series of platinum(II) Schiff Base salicylaldimine complexes (**Pt1**–**Pt9**) was synthesized with hydrogen, fluorine and methyl substituents on various positions on the phenyl rings of the backbone. The effect of electron withdrawing and donating substituents on the absorption and emission properties was investigated. These Pt(II) complexes show intense visible light absorption between 400 and 600 nm due to metal-to-ligand-charge-transfer (MLCT). Interestingly, the complexes showed viscosity and polarity-dependent strong emission upon green light excitation. **Pt1**–**Pt9 s**howed excellent photo-stability under continuous light irradiation and generated singlet oxygen with a quantum yield of ca. 50%.

In the dark, all the complexes were non-toxic to A549 lung cancer cells. However, strong photo-toxicity was observed after excitation with low-dose green light (520 nm, 7.02 J cm^{-2}). Cell imaging indicated that the complexes mostly localized in the cytoplasm,

Please cite this article as: S. Banerjee, M. S. Capper, G. J. Clarkson et al., Dual-action platinum(II) Schiff base complexes: Photocytotoxicity and cellular imaging, Polyhedron, https://doi.org/10.1016/j.poly.2019.04.024

targeting mitochondria and lysosomes efficiently. In general, this new series of green-light-activated Pt(II) Schiff base complexes has potential as photosensitizers for photodynamic therapy with mitochondria- and lysosome-targeting ability. The Pt(II) complexes show anticancer activity only upon light irradiation while remaining dormant in the dark. All these properties indicate that the complexes have the potential to overcome the problems of drug resistance and side effects of current clinical Pt(II) drugs.

Acknowledgements

We thank the EPSRC (grants EP/G006792, EP/F034210/1 and EP/P030572/1 for P.J.S.,), MRC (grant G0701062 for P.J.S.), The Royal Society (Newton-Bhahba International Fellowship NF151429 for S.B. and Newton International Fellowship NF160307 and Sun Yat-sen University Startup funding 75110-18841213 for H.H.). We thank Dr. L. Song and P. Aston for assistance with mass spectrometry; Dr. J. P. C. Coverdale and H. E. Bridgewater for assistance with ICP experiments; and Dr. I. Prokes for assistance with NMR spectroscopy.

Dedication

This paper is dedicated to Professor Akhil R. Chakravarty on the occasion of his 65th birthday.

Competing interests

The authors declare no competing financial interests.

Appendix A. Supplementary data

CCDC 1888366 and 1888367 contains the supplementary crystallographic data for **Pt5** and **Pt9**, respectively. These data can be obtained free of charge via http://www.ccdc.cam.ac.uk/conts/retrieving.html, or from the Cambridge Crystallographic Data Centre, 12 Union Road, Cambridge CB2 1EZ, UK; fax: (+44) 1223-336-033; or e-mail: deposit@ccdc.cam.ac.uk.

Supplementary data (crystallographic data for complexes **Pt5** and **Pt9**, 1D and 2D COSY ^{1}H NMR spectra for **Pt7**, and cyclic voltammograms for **Pt1**–**Pt9**) to this article can be found online at https://doi.org/10.1016/j.poly.2019.04.024.

References

[1] D.E. Dolmans, D. Fukumura, R.K. Jain, Nat Rev. Cancer 3 (2003) 380.
[2] B.W. Henderson, T.J. Dougherty, Photochem. Photobiol. 55 (1992) 145.
[3] Z. Zhou, J. Song, L. Nie, X. Chen, Chem. Soc. Rev. 45 (2016) 6597.
[4] D. Nowis, M. Makowski, T. Stokłosa, M. Legat, T. Issat, J. Gołąb, Acta Biochim. Pol. 52 (2005) 339.
[5] H.I. Pass, J. Natl, Cancer I (85) (1993) 443.
[6] S.B. Brown, E.A. Brown, I. Walker, Lancet Oncol. 5 (2004) 497.
[7] M. Ethirajan, Y. Chen, P. Joshi, R.K. Pandey, Chem. Soc. Rev. 40 (2011) 340.
[8] F. Heinemann, J. Karges, G. Gasser, Acc. Chem. Res. 50 (2017) 2727.
[9] A.E. O'Connor, W.M. Gallagher, A.T. Byrne, Photochem. Photobiol. 85 (2009) 1053.
[10] O. Mazor, A. Brandis, V. Plaks, E. Neumark, V. Rosenbach-Belkin, Y. Salomon, A. Scherz, Photochem. Photobiol. 81 (2005) 342.
[11] M. Price, L. Heilbrun, D. Kessel, Photochem. Photobiol. 89 (2013) 683.
[12] H. Huang, B. Yu, P. Zhang, J. Huang, Y. Chen, G. Gasser, L. Ji, H. Chao, Angew. Chem. Int. Ed. 54 (2015) 14049.
[13] Z. Lv, H. Wei, Q. Li, X. Su, S. Liu, K.Y. Zhang, W. Lv, Q. Zhao, X. Li, W. Huang, Chem. Sci. 9 (2018) 502.
[14] P. Zhang, C.K.C. Chiu, H. Huang, Y.P.Y. Lam, A. Habtemariam, T. Malcomson, M. J. Paterson, G.J. Clarkson, P.B. O'Connor, H. Chao, P.J. Sadler, Angew. Chem. Int. Ed. 56 (2017) 14898.
[15] L.K. McKenzie, H.E. Bryant, J.A. Weinstein, Coord. Chem. Rev. 379 (2019) 2.
[16] H. Huang, S. Banerjee, P.J. Sadler, ChemBioChem 19 (2018) 1574.
[17] S. Monro, K.L. Colon, H. Yin, J. Roque III, P. Konda, S. Gujar, R.P. Thummer, L. Lilge, C.G. Cameron, S.A. McFarland, Chem. Rev. 119 (2019) 797.
[18] E. Wong, C.M. Giandomenico, Chem. Rev. 99 (1999) 2451.
[19] T.C. Johnstone, K. Suntharalingam, S.J. Lippard, Chem. Rev. 116 (2016) 3436.
[20] J.S. Butler, P.J. Sadler, Curr. Opin. Chem. Biol. 17 (2013) 175.
[21] M. Obata, S. Hirohara, R. Tanaka, I. Kinoshita, K. Ohkubo, S. Fukuzumi, M. Tanihara, S. Yano, J. Med. Chem. 52 (2009) 2747.
[22] J. Deng, J. Wang, M. Khan, P. Yu, F. Yang, H. Liang, J. Inorg. Biochem. 185 (2018) 10.
[23] F.U. Rahman, A. Ali, H.-Q. Duong, I.U. Khan, M.Z. Bhatti, Z.-T. Li, H. Wang, D.-W. Zhang, Eur. J. Med. Chem. 164 (2019) 546.
[24] T. Chatzisideri, S. Thysiadis, S. Katsamakas, P. Dalezis, I. Sigala, T. Lazarides, E. Nikolakaki, D. Trafalis, O.A. Gederaas, M. Lindgren, V. Sarli, Eur. J. Med. Chem. 141 (2017) 221.
[25] C.M. Che, C.C. Kwok, S.W. Lai, A.F. Rausch, W.J. Finkenzeller, N. Zhu, H. Yersin, Chem. Eur. J. 16 (2010) 233.
[26] S.S. Razi, Y.H. Koo, W. Kim, W. Yang, Z. Wang, H. Gobeze, F. D'Souza, J. Zhao, D. Kim, Inorg. Chem. 57 (2018) 4877.
[27] J. Zhang, L. Xu, W.Y. Wong, Coord. Chem. Rev. 355 (2018) 180.
[28] J. Zhang, G. Dai, F. Wu, D. Li, D. Gao, H. Jin, S. Chen, X. Zhu, C. Huang, D. Han, J. Photochem. Photobiol. A 316 (2016) 12.
[29] O.V. Dolomanov, L.J. Bourhis, R.J. Gildea, J.A.K. Howard, H. Puschmann, J. Appl. Cryst. 42 (2009) 339.
[30] G.M. Sheldrick, Acta Cryst. A71 (2015) 3.
[31] G.M. Sheldrick, Acta Cryst. C71 (2015) 3.
[32] C.K. Prier, D.A. Rankic, D.W. MacMillan, Chem. Rev. 113 (2013) 5322.
[33] C. Mari, V. Pierroz, R. Rubbiani, M. Patra, J. Hess, B. Spingler, L. Oehninger, J. Schur, I. Ott, L. Salassa, S. Ferrari, G. Gasser, Chem. Eur. J. 20 (2014) 14421.
[34] D. Babic, M. Čurić, K. Molčanov, G. Ilc, J. Plavec, Inorg. Chem. 47 (2008) 10446.
[35] V. Shanmugam, S. Selvakumar, C.S. Yeh, Chem. Soc. Rev. 43 (2014) 6254.
[36] M.K. Kuimova, S.W. Botchway, A.W. Parker, M. Balaz, H.A. Collins, H.L. Anderson, K. Suhling, P.R. Ogilby, Nat. Chem. 1 (2009) 69.
[37] T. Goslinski, J. Piskorz, J. Photochem. Photobiol. C 12 (2011) 304.
[38] T.J. Dougherty, Photochem. Photobiol. 58 (1993) 895.
[39] D. Wang, S.J. Lippard, Nat. Rev. Drug Discov. 4 (2005) 307.
[40] D. Fink, S. Nebel, S. Aebi, H. Zheng, B. Cenni, A. Nehmé, R.D. Christen, S.B. Howell, Cancer Res. 56 (1996) 4881.